Dyes and Pigments 125 (2016) 36–43

Contents lists available at ScienceDirect

Dyes and Pigments

journal homepage: www.elsevier.com/locate/dyepig

Film-forming hole transporting materials for high brightness flexible organic light-emitting diodes

Xicheng Liu [a, b], Jing You [a, b, *], Yin Xiao [a, b], Shirong Wang [a, b], Wenzheng Gao [c], Junbiao Peng [d, e], Xianggao Li [a, b]

[a] School of Chemical Engineering and Technology, Tianjin University, Tianjin 300072, China
[b] Collaborative Innovation Center of Chemical Science and Engineering (Tianjin), Tianjin 300072, China
[c] Technical Institute of Physics and Chemistry, Chinese Academy of Sciences, Beijing 100190, China
[d] Institute of Polymer Optoelectronic Materials and Devices, South China University of Technology, Guangzhou 510640, China
[e] Key Laboratory of Specially Functional Materials and Advanced Manufacturing Technology, Ministry of Education, Guangzhou 510640, China

ARTICLE INFO

Article history:
Received 9 August 2015
Received in revised form
29 September 2015
Accepted 1 October 2015
Available online xxx

Keywords:
Film-forming
Triphenylamine
Hole transporting materials
Flexible organic light-emitting diodes
High brightness
Solution-processable

ABSTRACT

Film-forming property of organic semiconductors is one of crucial factors for the performance of flexible organic light-emitting diode. In this work, two hole transporting materials based on triphenylamine were synthesized, which showed an outstanding film-forming property and could form free-standing films with a diameter of 4 mm. The spin-coated films on the flexible substrates showed an unobvious mechanical failure bended with radius of curvature no less than 6 mm. Photoelectron yield spectroscopy show that the two compounds embody suitable highest occupied molecular orbital levels (−5.14 eV and −5.25 eV) for hole injection. The sandwiched organic light-emitting diodes use poly[2-(4-3′,7′-dimethyloctyloxy)-phenyl]-*p*-phenylenevinylene) as emitting and electron transporting layer showed higher stability with increasing operation current density, an maximum luminance level of 103,690 cd m^{-2}. It demonstrate that the as-synthesized hole transporting materials hold a promising in high brightness flexible organic light-emitting diodes.

© 2015 Elsevier Ltd. All rights reserved.

1. Introduction

Flexible organic light-emitting devices (FOLEDs) as next generation displayer not only can be used in full-color flexible flat-panel displays and solid-state lighting, but also overture the traditional interactive mode with computers [1–5]. The OLEDs were started with simple sandwich structure [6]. In order to balance the hole and electron injection and transition in device, the hole/electron injection layers, hole/electron barrier layers were introduced [7–11]. To date, most of OLEDs are fabricated with layer-by-layer evaporation process to form the high quality ultra-thin films. However, this technique still has problems such as requirement of expensive equipment, high cost and low material utilization [12,13]. Recently, the solution processing techniques such as spin-coating, inject printing and spray coating were proposed to realize FOLED cheaply and conveniently [14]. While, the commercialized small molecular hole transporting materials (HTMs) such as 1,4-bis(1-naphthylphenyl) amino)biphenyl (NPB) and *N*,*N*′-bis(3-methylphenyl)-1,10-biphenyl-4,4′-diamine (TPD) does not fit for solution process due to the low glass transition temperature (NPB: $T_g \approx 99$ °C, TPD: $T_g \approx 50$ °C) [15].

At present, in FOLEDs the hole transporting layer mainly use the water-dispersible conducting polymer poly(3,4-ethylene-dioxythiophene) poly(styrene sulfonate) (PEDOT:PSS) with spin-coating process [16,17]. However, the acid of PEDOT:PSS will corrode the ITO leading to the unstable of OLEDs during operation at high current density [18]. In addition, the accumulation of excitons at the interface of PEDOT:PSS and emitting layer resulted in the decrease of interfacial luminescence quantum yield [19].

In this work, we designed and synthesized two hole transporting materials *N*,*N*-di(phenyl)-*N*′,*N*′-di(4-(4-*N*,*N*-di(4-benzyl)amino) phenyl)ethenyl)-1,1′-biphenyl-4,4′-diamine (*p*-(TPA-Et)$_4$-TPB) and *N*,*N*,*N*′,*N*′-tetra(4-(4-*N*,*N*-di(4-benzyl)amino)phenyl) ethenyl)-1,1′-biphenyl-4,4′-diamine (*p*-(TPA-BD)$_2$-TPA) to replace the PEDOT:PSS layer in the all solution processing OLEDs. The molecular structures are shown in Scheme 1. Here, TPA moieties are connected with

* Corresponding author. School of Chemical Engineering and Technology, Tianjin University, Tianjin 300072, China. Tel.: +86 22 2740 4208.
E-mail address: Youj1983@tju.edu.cn (J. You).

http://dx.doi.org/10.1016/j.dyepig.2015.10.004
0143-7208/© 2015 Elsevier Ltd. All rights reserved.

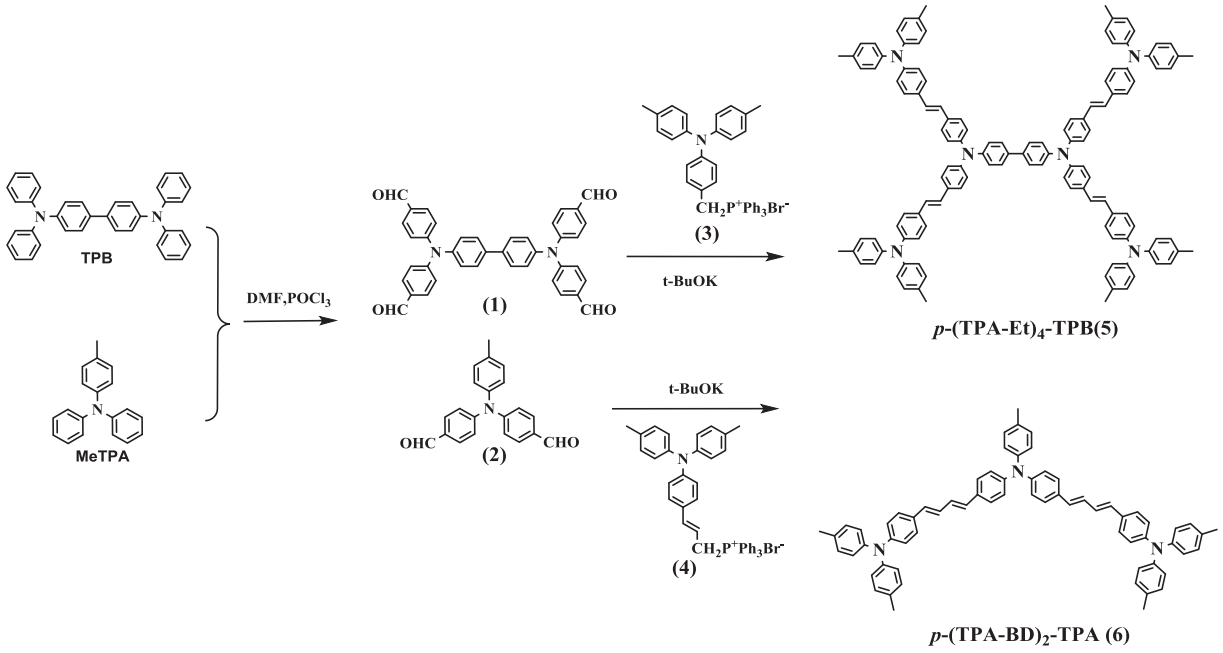

Scheme 1. The synthetic procedure of *p*-(TPA-Et)$_4$-TPB (**5**) and *p*-(TPA-BD)$_2$-TPA (**6**).

ethane (for *p*-(TPA-Et)$_4$-TPB) or butadiene (for *p*-(TPA-BD)$_2$-TPA) to modify the HOMO levels and improve the morphology during spin-coating [20]. The OLEDs with as-synthesized HTMs have been fabricated by all solution processing with poly(2-(4-ethylexyl) phenyl-1,4-phenylenevinylene (p-PPV) as electron transporting and emitting layer [21]. The OLEDs with as-synthesized HTMs showed an improvement on maximum luminance (L_{max}) and turn-on voltage (V_{onset}), as well as the stability at high operation current compared with the OLED using PEDOT:PSS. The OLEDs based on *p*-(TPA-Et)$_4$-TPB showed L_{max} of 103,690 cd m^{-2}, which was much larger than OLEDs based on PEDOT:PSS (L_{max} of 55,219 cd m^{-2}). It demonstrates the as-synthesized HTMs hold a promising in high brightness flexible OLEDs.

2. Experimental

2.1. Materials and methods

N,*N*,*N*′,*N*′-tetraphenyl-[1,1′-biphenyl]-4,4′-diamine (TPB), 4-methyl-*N*,*N*-diphenylaniline (MeTPA), Poly(3,4-ethylenedioxy-thiophene):poly(styrene-sulfonate) (PEDOT:PSS), Barium (Ba, 137.33, 99.9%) and Aluminum (Al, 26.98, 99%) were purchased from Tianjin Heowns Biochemical Technology Co. LTD., poly[2-(4-3′,7′-dimethyloctyloxy)-phenyl]-*p*-phenylenevinylene) (p-PPV) was provided by South China University of Technology. ITO glass was purchased from South China Xiangcheng technology Co. LTD., other reagents were purchased from Tianjin Guangfu Fine Chemical Research Institute. *N*,*N*-dimethyl formamide (DMF), Phosphorus oxychloride ($POCl_3$), Tetrahydrofuran (THF) were freshly distilled before use.

As-synthesized HTMs were identified by NMR spectra, FT-IR spectra, mass spectroscopy (MS) and elemental analysis. Fourier transfer infrared spectra (FT-IR) were measured as a KBr disk on a Thermo NICOLET380 spectrometer. Nuclear magnetic resonance (NMR) spectra was obtained on a Varian INOVA 400, 500 MHz spectrometer, with the chemical shifts reported in ppm using tetramethylsilane (TMS) as an internal standard. Mass spectra (MS) were recorded on a Thermo FINNIGAN LCQ Advantage mass spectrometer. Elemental analysis was performed on a VarioMICRO CHNOS elemental analyzer. Decomposition temperature (T_d) and glass transition temperature (T_g) were determined under a nitrogen atmosphere at a heating rate of 10 °C min^{-1} by the thermo gravimetric analysis (TGA) and differential scanning calorimeter (DSC) on a TA Q500 thermo gravimetric analysis and TA Q20 thermal analysis. Ultraviolet–visible absorption (UV–Vis) spectroscopy and photoluminescence (PL) spectra were measured by the Thermo Evolution 300 UV–visible spectrometer and a Cary Eclipse fluorescence spectrometer, respectively. The thickness of spin-coating films was measured by a TencorAlfa Step-500 terrace detector. The photoelectron yield spectroscopy (PYS) was carried out on a Sumitomo PYS-202 Ionization energy detection system. The morphology of solid films were characterized by a Rigaku Miniflex 600 X-Ray diffraction (XRD) and Nanosurf AG Easyscan 2 atomic force microscopy (AFM). The carrier mobility was measured on Sumitomo TOF401 TOF measurement system. The topography of thin films under different curvature radius was obtained by Hitachi S-4800 field emission scanning electron microscopy (FESEM).

2.2. Synthesis

The designed synthetic route for *p*-(TPA-Et)$_4$-TPB and *p*-(TPA-BD)$_2$-TPA are depicted in Scheme 1.

2.2.1. Synthesis of *N*,*N*,*N*′,*N*′- tetra(4-formylphenyl)-1,1′-biphenyl-4,4′-diamine (*1*)

DMF (45 mmol) was weighed into a 100 mL round-bottom flask, under the protection of nitrogen (N_2). Then, $POCl_3$ (45 mmol) was added dropwise into above flask, stirred for 1 h at 0 °C. After that, TPB 1,2-dichloroethane solution (4.5 mmol, 0.225 mol L^{-1}) was added dropwise into above solution at room-temperature, then stirred for another 34 h at 95 °C. The reaction was stopped by ice water. The compound **1** was purified by chromatographed on a silica gel column (petroleum ether: ethyl acetate = 15:1 as eluent) with yield of 8% (0.21 g): Mp: 181–182 °C; ^{1}H NMR (500 MHz, $CDCl_3$) δ (ppm): 9.930 (s, 4H), 7.080 (d, J = 9.0 Hz, 4H), 7.209–7.240 (m, 12H), 7.381 (d, J = 9.0 Hz, 4H), 9.823 (s, 4H); MS (*m/z*): Found 601.4 [M$^+$], Calcd. for $C_{40}H_{28}N_2O_4$:[(M + H)$^+$], 601.2.

*2.2.2. Synthesis of 4-N,N-di(4-formylphenyl)tolylbenzenamine (**2**)*

Compound **2** was synthesized according to the method described in 2.2.1 with yield of 39%: Mp: 145–146 °C; ^{1}H NMR (500 MHz, $CDCl_3$) δ (ppm): 2.365 (s, 3H), 7.061 (d, J = 8.0 Hz, 2H), 7.203 (d, J = 8.5 Hz, 2H), 7.168 (d, J = 8.5 Hz, 4H), 7.755 (d, J = 8.5 Hz, 4H), 9.886 (s, 2H); MS (*m/z*): Found 316.8 [M^+], Calcd. for $C_{21}H_{17}NO_2$: [$(M + H)^+$], 316.4.

*2.2.3. Synthesis of 4-[N,N′-di-(p-tolyl)amino]benzyl(triphenyl) phosphonium bromide (**3**)*

Compound **3** was synthesized according to literature [20] with yield of 96%: Mp: 231–233 °C; ^{1}H NMR (500 MHz, $CDCl_3$) δ (ppm): 2.254 (s, 6H), 5.314 (s, 2H), 6.730 (d, J = 8.5 Hz, 2H), 6.844 (d, J = 9.0 Hz, 2H), 6.896 (d, J = 9.0 Hz, 4H), 7.031 (d, J = 9.0 Hz, 4H), 7.622–7.782 (m, 15H); MS (*m/z*): Found 548.1 [$(M-Br)^+$], Calcd. for $C_{39}H_{35}BrNP$: [$(M-Br)^+$], 548.3.

*2.2.4. Synthesis of 1-{4-[N,N-di(p-tolyl)amino]phenyl} allyl(triphenyl) phosphonium bromide (**4**)*

Compound **4** was synthesized according to literature [20] with yield of 97%: Mp: 111–113 °C; ^{1}H NMR (500 MHz, $CDCl_3$) δ (ppm): 2.304 (s, 6H), 4.970 (d, J = 15.0 Hz, 2H), 6.836 (d, J = 8.5 Hz, 2H), 6.950–7.062 (m, 12H), 7.663–7.904 (m, 15H). MS (*m/z*): Found 573.3 [$(M-Br)^+$], Calcd. for $C_{41}H_{37}BrNP$: [$(M-Br)^+$], 573.3.

*2.2.5. Synthesis of N,N-di(phenyl)-N′,N′-di(4-(4-N,N-di(4-benzyl) amino) phenyl)ethenyl)-1,1′-biphenyl-4,4′-diamine (p-(TPA-Et)$_4$-TPB, **5**)*

Compound **1** (0.30 g, 0.5 mmol) and **3** (2.52 g, 4 mmol) synthesized above were added into a 100 mL round-bottom flask with protection of N_2. Anhydrous THF (20 mL) was added to above flask, then cooled to 0 °C. The THF solution of t-BuOK (16 mmol, 0.8 mol L^{-1}) was added dropwise to above flask, stirred for 30 min at 0 °C, followed with stirred at room temperature until the compound **1** was consumed completely (monitored by thin-layer chromatography). The reaction was terminated with ice water. The crude product was heated under reflux for 8 h in THF with a catalytic amount of iodine. Then the remaining iodine was removed by sodium hydroxide (NaOH) solution (Wt = 10%, 100 mL) with stirring for 2 h. After that, the product was purified by chromatographed on a silica gel column (petroleum ether: ethyl acetate = 50:1 as eluent) to give the title compound as a pure *E* stereoisomer *p*-(TPA-Et)$_4$-TPB (0.61 g, 73%): IR (cm^{-1}, KBr): 2928, 2853, 1603, 1500, 1321, 964, 823; ^{1}H NMR (400 MHz, $CDCl_3$) δ 7.51 (d, J = 8.6 Hz, 4H), 7.41 (d, J = 8.6 Hz, 8H), 7.36 (d, J = 8.7 Hz, 8H), 7.20 (d, J = 8.5 Hz, 4H), 7.07 (ddd, J = 30.4, 17.4 Hz, 11.7 Hz, 56H), 2.35 (s, 24H); MS (*m/z*): Found 1677.437 [M^+], Calcd. for $C_{124}H_{104}N_6$: [$(M + H)^+$], 1677.836. Elemental analysis: Found: C, 88.73; N, 5.04; H, 6.23%, Calcd. for $C_{124}H_{104}N_6$: C, 88.75; N, 5.01; H, 6.25%.

*2.2.6. Synthesis of N,N,N′,N′-tetra(4-(4-N,N-di(4-benzyl)amino) phenyl) ethenyl)-1,1′-biphenyl-4,4′-diamine (p-(TPA-BD)$_2$-TPA, **6**)*

p-(TPA-BD)$_2$-TPA (**6**) was synthesized according to the method described above with yield of 57%: IR (cm^{-1}, KBr): 2910, 1597, 1500, 1322, 967, 807; ^{1}H NMR (400 MHz, $CDCl_3$) δ 7.30–7.23 (m, 8H), 7.11–6.93 (m, 28H), 6.87–6.77 (m, 4H), 6.59–6.51 (m, 4H), 2.33 (s, 3H), 2.31 (s, 12H); MS (*m/z*): Found 905.840 [M^+], Calcd. for $C_{67}H_{59}N_3$: [$(M + H)^+$], 905.471. Elemental analysis: Found: C, 88.83; N, 4.62; H, 6.55%, Calcd. for $C_{67}H_{59}N_3$: C, 88.80; N, 4.64; H, 6.56%.

2.3. Fabrication of free-standing films

The free-standing films were obtained on the air–water interface with Langmuir–Blodgett (LB) method. The π–A curves are shown in ESI Fig. S1. Isotherms at the air–water interface were recorded using a 80 mm × 210 mm × 8 mm (W*L*H) PTFE Langmuir trough equipped with a compression barrier and a floating barrier for the detection of surface pressure *via* the Langmuir method (POWEREACH JML04C1, China). The as-synthesized HTMs were spread from CH_2Cl_2 solution with 0.5 wt%. LB transfer was made by the horizontal method described in the literature [22]. The films were compressed to 45 mN m^{-1} before transfer was carried out.

2.4. Fabrication of electroluminescent devices

Multilayer light-emitting diodes, with a configuration of ITO/PEDOT: PSS/Alq_3/LiF/Al were fabricated for the investigation of optoelectronic characteristics. ITO-coated substrates (sheet resistance: 10 Ω sq^{-1}) was cleaned with following sequence: in acetone, methanol, and diluted water [23]. After that, the substrates were annealing at 120 °C for 20 min followed by O_2 plasma treatment. PEDOT:PSS colloidal solution was spin-coated on the ITO (2000 rpm), then annealed at 60 °C for 30 min to give HTL with thickness <100 nm. p-PPV chlorobenzene solution (0.9 wt%) was spin-coated on the top of HTL layer (2500 rpm), then annealed at 80 °C for 20 min to give a EL with thickness of 80 nm. The Ba (3 nm) and Al (100 nm) layers were thermally deposited as a cathode under vacuum ($P < 1 \times 10^{-4}$ Pa). Device-*p*-(TPA-BD)$_2$-TPA and device-*p*-(TPA-Et)$_4$-TPB were fabricated with same procedures only replay the PEDOT:PSS colloidal solution with *p*-(TPA-BD)$_2$-TPA and *p*-(TPA-Et)$_4$-TPB THF solution (1 wt%). FOLEDs with *p*-(TPA-BD)$_2$-TPA and PEDOT as HTL were fabricated with same procedure. The EL spectra were measured by a Photo Research SpectrScan PR705 spectra. Steady current density *versus* bias, luminance *versus* bias were measured by a combination of a Keithley 236 with silicon photodiode and a Photo Research PR705 spectra. All tests were performed under air atmosphere and at room temperature.

3. Results and discussion

3.1. Characterization of p-(TPA-Et)$_4$-TPB and p-(TPA-BD)$_2$-TPA

The synthetic routes of *p*-(TPA-Et)$_4$-TPB (5) and *p*-(TPA-BD)$_2$-TPA (6) are shown in Scheme 1. *N,N,N′,N′*-tetra(4-formylphenyl)-1,1′-biphenyl-4,4′-diamine (1), 4-*N,N*-di(4-formylphenyl)tolylbenzen-amine (2), 4-[*N,N′*-di-(p-tolyl)amino]benzyl (triphenyl)phosphonium bromide (3) and 1-{4-[*N,N*-di(p-tolyl)amino]phenyl} allyl(triphenyl)phosphonium bromide (4) were prepared according to the procedures reported previously [23]. The *p*-(TPA-Et)$_4$-TPB was synthesized from compound (1) and compound (3), by Wittig reaction in 73% yield. The *p*-(TPA-BD)$_2$-TPA was synthesized from compound (2) and compound (4) in 57% yield with the same method. The structure of *p*-(TPA-Et)$_4$-TPB and *p*-(TPA-BD)$_2$-TPA were confirmed *via* FT-IR, ^{1}H NMR, MS and elemental analysis, which agreed well with the proposed molecular structure (See ESI Fig. S2, Fig. S3).

The as-synthesized HTMs are soluble in common used organic solvents such as toluene, tetrahydrofuran (THF), chloroform and chlorobenzene, which is ensure they can deposited with solution processing technique [24]. This result is probably due to the presence of methyl substituents on the TPA moieties and the non-planar molecular structure.

3.2. Thermal properties

The decomposition temperatures (T_d, which corresponds to the temperature to decomposition of 5%) of as-synthesized HTMs were

measured by thermal gravimetric analysis (TGA) at the heating rate of 10 °C min^{-1} under N_2. Both *p*-(TPA-Et)$_4$-TPB and *p*-(TPA-BD)$_2$-TPA showed T_d ~300 °C (298.9 °C for *p*-(TPA-BD)$_2$-TPA; 303.6 °C for *p*-(TPA-Et)$_4$-TPB) which indicated the excellent thermal stability (See ESI Fig. S4). The glass-transition temperatures (T_g) were determined by differential scanning calorimetry (DSC) according to the following procedure: the sample was heated to 250 °C at the rate of 10 °C min^{-1}, then cooled to 0 °C, after that scan from 0 to 250 °C at a rate of 10 °C min^{-1}. As shown in Fig. 1, T_g of *p*-(TPA-Et)$_4$-TPB and *p*-(TPA-BD)$_2$-TPA are determined to be 138.3 °C and 169.2 °C, respectively. The higher T_g of *p*-(TPA-Et)$_4$-TPB was due to the larger molecular weight [25].

3.3. Optical properties

The normalized UV–Vis absorption and photoluminescence (PL) spectra of as-synthesized HTMs in THF solution (1.0×10^{-5} mol L^{-1}) and spin-coated films are shown in Fig. 2, relevant data are summarized in Table 1. As shown in Fig. 2, *p*-(TPA-Et)$_4$-TPB and *p*-(TPA-BD)$_2$-TPA show two absorption bands at 300–310 nm and 400–450 nm. The absorption bands in 300–310 nm region can be assigned to the n–π* transition of the TPA moieties. The absorption peaks in 400–450 nm attribute to the intramolecular charge transfer (ICT) of π–π* transition.

Compared with *p*-(TPA-Et)$_4$-TPB, the red-shift (25 nm) of π–π* ICT bands mainly result from the extension of the π–π conjugated by butadiene group of *p*-(TPA-BD)$_2$-TPA [20]. Compared the UV–Vis absorption and PL spectra of THF solutions and thin films, we can find that in *p*-(TPA-Et)$_4$-TPB the shape and peak position are similar. No obvious red-shift of absorption peaks indicated that no significant aggregation or crystallization occurs in the films [26]. In films, the PL peak slightly widen due to the intermolecular interaction for both *p*-(TPA-Et)$_4$-TPB and *p*-(TPA-BD)$_2$-TPA.

3.4. Ionization potentials

The photoelectron yield spectroscopy (PYS) method as a new tool to study the energy distribution of electronic states can determine the ionization potential (E_{IP}) directly [27]. Mechanism of PYS method is shown in ESI Fig. S5. The PYS of spin-coating films are shown in Fig. 3.

As shown in Fig. 3, the threshold energies refer to the E_{IP} of thin films spin-coating with as-synthesized HTMs. The HOMO levels are

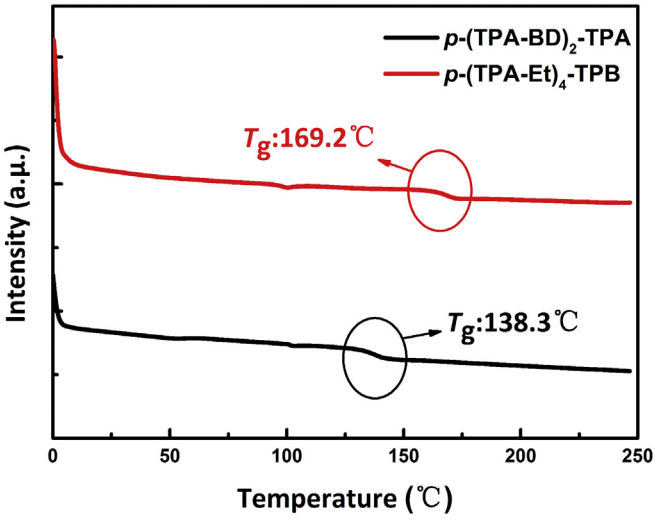

Fig. 1. DSC curves of as-synthesized HTMs at a heating rate of 10 °C min^{-1} under N_2.

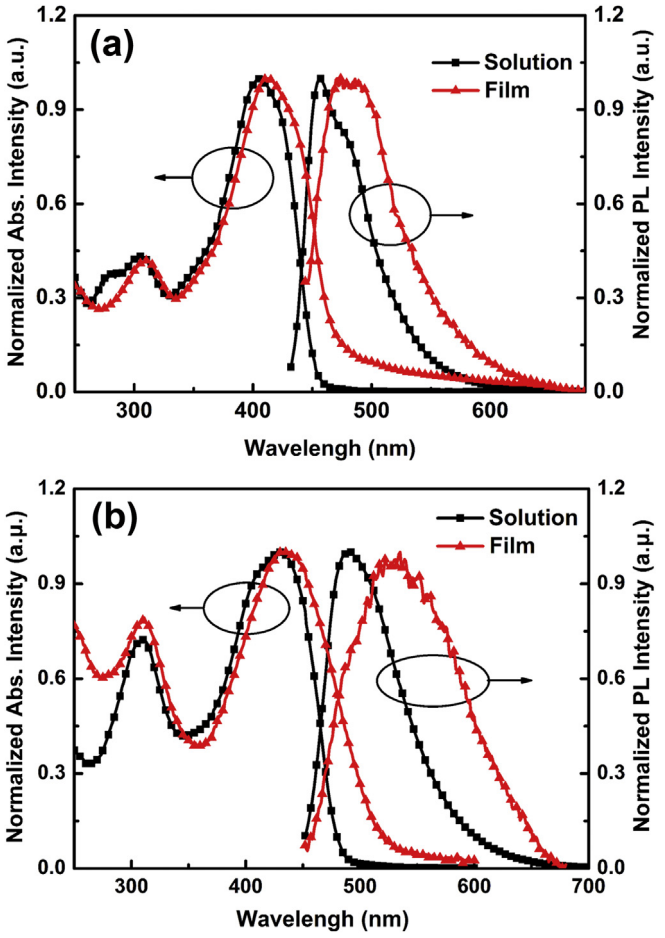

Fig. 2. Normalized UV–Vis absorption and PL spectra: (a) *p*-(TPA-Et)$_4$-TPB; (b) *p*-(TPA-BD)$_2$-TPA (THF solution, 1.0×10^{-5} mol L^{-1}).

determined as the minus of E_{IP}, which are −5.14 eV (*p*-(TPA-Et)$_4$-TPB) and −5.25 eV (*p*-(TPA-BD)$_2$-TPA), respectively [28]. The HOMO level of PEDOT:PSS thin films is reported to be −5.20 eV [29]. This indicated that the as-synthesized HTMs hold the promise to replace the PEDOT:PSS layer as HTL. The HOMO levels of *p*-(TPA-Et)$_4$-TPB and *p*-(TPA-BD)$_2$-TPA are similar due to the same electron donor group (TPA moieties). The LUMO level of *p*-(TPA-Et)$_4$-TPB is much higher than *p*-(TPA-BD)$_2$-TPA film, which indicated that the butadiene units have stronger ability to increase conjugation in molecule than ethane units [30].

3.5. Film-forming properties

Morphological property is a crucial factor determines the performance of solution-processable OLEDs. Distinct crystallization in films will suppress the exciton generation and transform which resulted in device deteriorate [31]. Morphologies of spin-coating films of as-synthesized HTMs were investigated with atomic force microscopy (AFM) and X ray diffraction (XRD) measurements. These results are shown in Fig. 4.

As shown in Fig. 4 (a, b), the surface root mean square (RMS) roughness of *p*-(TPA-BD)$_2$-TPA and *p*-(TPA-Et)$_4$-TPB films are 0.401 nm and 0.546 nm respectively. This indicated that the surface smoothness of spin-coating films are better than PEDOT:PSS spin-coating films which reported to be 0.685 nm [32]. The amorphous properties of *p*-(TPA-Et)$_4$-TPB and *p*-(TPA-BD)$_2$-TPA films

Table 1
The optical, thermal properties and energy levels of as-synthesized HTMs.

	T_d[a] (°C)	T_g[b] (°C)	λ_{abs}[c] (nm)	λ_{onset}[c] (nm)	PL[d] (nm)	E_g[e] (eV)	HOMO[f] (eV)	LUMO[g] (eV)
p-(TPA-Et)$_4$-TPB	303.6	169.2	305, 406/309, 414[h]	455	456/471[h]	2.73	−5.14	−2.41
p-(TPA-BD)$_2$-TPA	298.9	138.3	311, 431/311, 439[h]	583	492/535[h]	2.13	−5.25	−3.12

[a] Measured by TGA at a heating rate of 10 °C min^{-1} under nitrogen atmosphere.
[b] Measured by DSC according to the heat–cool–heat procedure.
[c] Absorption spectra were recorded in the 1.0 × 10^{-5} mol L^{-1} THF solution.
[d] PL spectra were recorded in the 1.0 × 10^{-5} mol L^{-1} THF solution, with excitation wavelength at maximum absorption shown in Fig. 2.
[e] Optical energy gaps calculated from the absorption thresholds from UV–Vis absorption spectra of films.
[f] Measured with PYS.
[g] |LUMO| = |HOMO|−|E_g|.
[h] Absorption peaks of thin films.

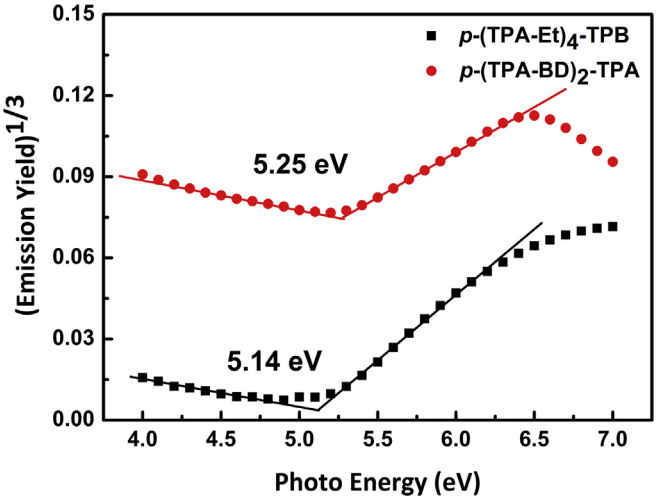

Fig. 3. Photoelectron yield spectroscopy curves of *p*-(TPA-BD)$_2$-TPA and *p*-(TPA-Et)$_4$-TPB.

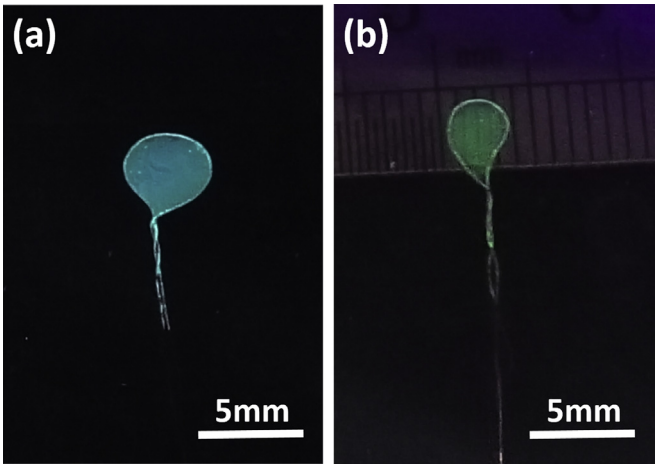

Fig. 5. Free-standing films obtained by LB technique: (a) *p*-(TPA-Et)$_4$-TPB; (b) *p*-(TPA-BD)$_2$-TPA.

were confirmed by the XRD curves in Fig. 4(c). These results indicate that the as-synthesized HTMs are suitable for solution process.

As show in Fig. 5, free-standing films of *p*-(TPA-BD)$_2$-TPA and *p*-(TPA-Et)$_4$-TPB were achieved for the first time. These films can be supported on the metal rings with diameter of 4 mm. The breakage is unobvious in both *p*-(TPA-BD)$_2$-TPA and *p*-(TPA-Et)$_4$-TPB free-standing films on the 4 mm rings. These free-standing films showed an emission of sky-blue (Fig. 5 (a)) and green (Fig. 5 (b)) light under irradiation of UV light, which is agreement with the fluorescence emission spectra of spin-coating films (Fig. 2 (b)). While using the same method, small molecular HTMs, for example: NPB and TPD could not form free-standing films.

The mechanical properties of spin-coating films of as-synthesized HTMs were investigated with method reported in literature [33]. Brief description is shown in ESI Fig. S6. Typically, the thickness of substrate is much larger than active layer (approximately 100–200 nm) in FOLEDs. Therefore, the thickness of active layer is negligible. The film strain (ε_f) and radius of curvature have the relationship as $\varepsilon_f = d/2R$ [33]. Here, d is thickness of substrate, R is radius of curvature.

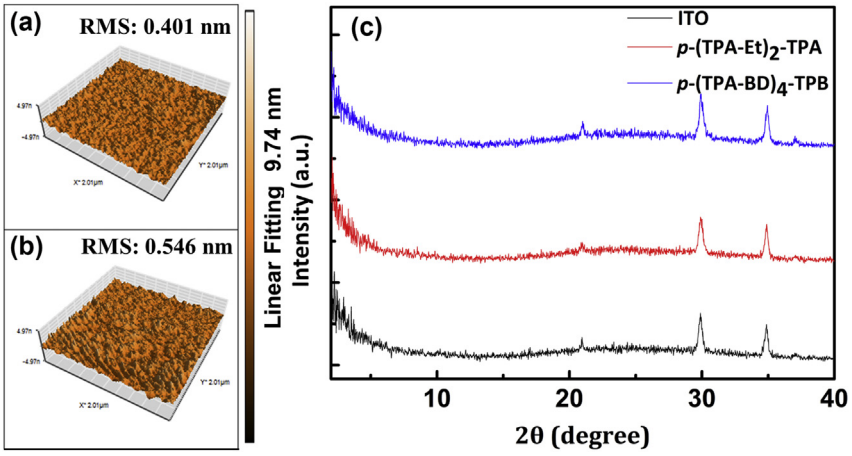

Fig. 4. The AFM images (a, b) and XRD curvature (c) of solid films: (a) *p*-(TPA-BD)$_2$-TPA RMS: 0.401 nm; (b) *p*-(TPA-Et)$_4$-TPB RMS: 0.546 nm.

The surface morphologies of spin-coating films of as-synthesized HTMs were measured by scan electronic microscope (SEM, Fig. 6). The SEM images of spin-coating films after bended with radius curvatures of 6 mm and 4 mm showed that, the fracture become obvious. Therefore, the ε_f values of spin-coating films of as-synthesized HTMs are in the region 0.024–0.021. It demonstrates that the as-synthesized HTMs are suitable for FOLED, which can be bend with radius curvature no less than 6 mm.

All above results demonstrate the outstanding film forming capability of as-synthesized HTMs.

3.6. Electroluminescent properties of solution processable OLEDs

The hole-injection and transporting properties of as-synthesized HTMs were evaluated with the OLEDs fabricated with spin-coating process. The device structure are ITO (185 nm)/HTM (70 nm)/p-PPV (80 nm)/Ba (3 nm)/Al (120 nm) as shown in Fig. 7 (a).

Here, poly[2-(4-3′,7′-dimethyloctyloxy)-phenyl]-*p*-phenylenevinylene (p-PPV) was used as emitting and electron transporting layer (E&ETL). The normalized electroluminance (EL) spectra were shown in Fig. 7 (b). All these devices show the EL peaks at the region of 500–550 nm, which are exclusive green emission of p-PPV layer. This indicated no exciplex formation at the interface of HTL/EML [21]. Compared with device-PEDOT and device-*p*-(TPA-Et)$_4$-TPB, the EL spectra of device *p*-(TPA-BD)$_2$-TPA only showed a emission peak at ~540 nm. As discussed above, the fluorescence emission peaks of *p*-(TPA-BD)$_2$-TPA film is ~535 nm. This phenomenon might be due to energy transfer from excited p-PPV to *p*-(TPA-BD)$_2$-TPA [34].

The current density–voltage–luminance (*J*–*V*–*L*) characteristics and current efficiency *vs.* current density curves of OLEDs are showing in Fig. 8, corresponding parameters are summarized in Table 2. As shown in Fig. 8 (a) and Table 2, the turn-on voltages (V_{onset}) of device-PEDOT is 3.75 V. With replacing HTL from PEDOT to *p*-(TPA-Et)$_4$-TPB and *p*-(TPA-BD)$_2$-TPA, the V_{onset} is decreased 0.25 V and 0.5 V, respectively. As shown in Table 1, the HOMO level of PEDOT, *p*-(TPA-Et)$_4$-TPB and *p*-(TPA-BD)$_2$-TPA are −5.30 eV, −5.14 eV and −5.25 eV, respectively (Fig. 9).

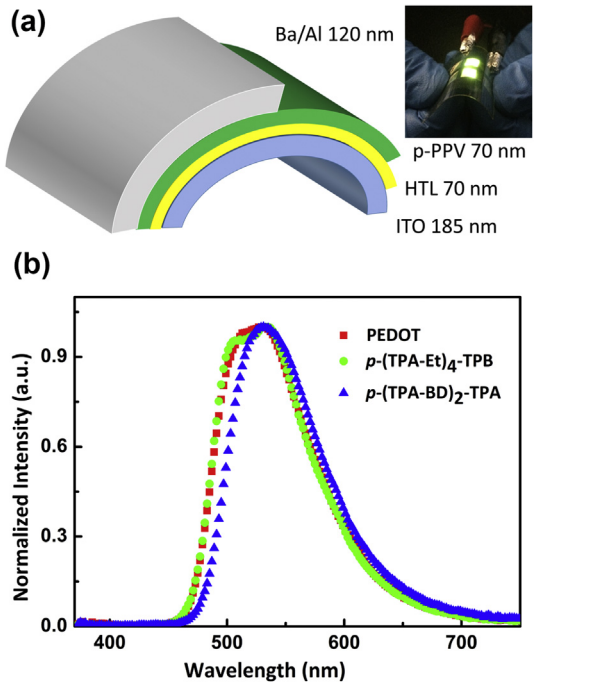

Fig. 7. Schematic of OLED structure (a) and EL spectra of PEDOT, *p*-(TPA-Et)$_4$-TPB and *p*-(TPA-BD)$_2$-TPA based OLEDs (b); Photograph of *p*-(TPA-Et)$_4$-TPB based FOLED (small image in (a)).

In order to estimate the effect of HOMO level on V_{onset}, we definite the injection barrier without bias voltage ($\triangle E_{inj}$) as the difference between ITO work function (−0.48 eV) and HOMO level of HTL (Table 2). Apparently, the smaller $\triangle E_{inj}$ lead to lower V_{onset} [35]. The lower V_{onset} demonstrate the outstanding hole injection capability of as-synthesized HTMs.

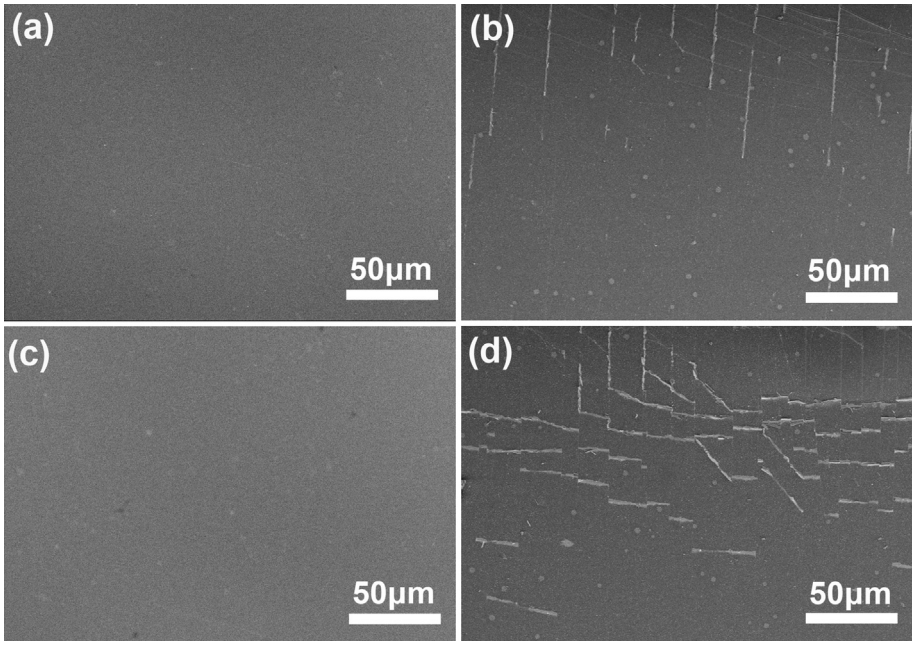

Fig. 6. The SEM map of flexural films of *p*-(TPA-Et)$_4$-TPB and *p*-(TPA-BD)$_2$-TPA: (a) *p*-(TPA-Et)$_4$-TPB, $R = 6$ mm; (b) *p*-(TPA-Et)$_4$-TPB, $R = 4$ mm; (c) *p*-(TPA-BD)$_2$-TPA, $R = 6$ mm; (d) *p*-(TPA-BD)$_2$-TPA, $R = 4$ mm.

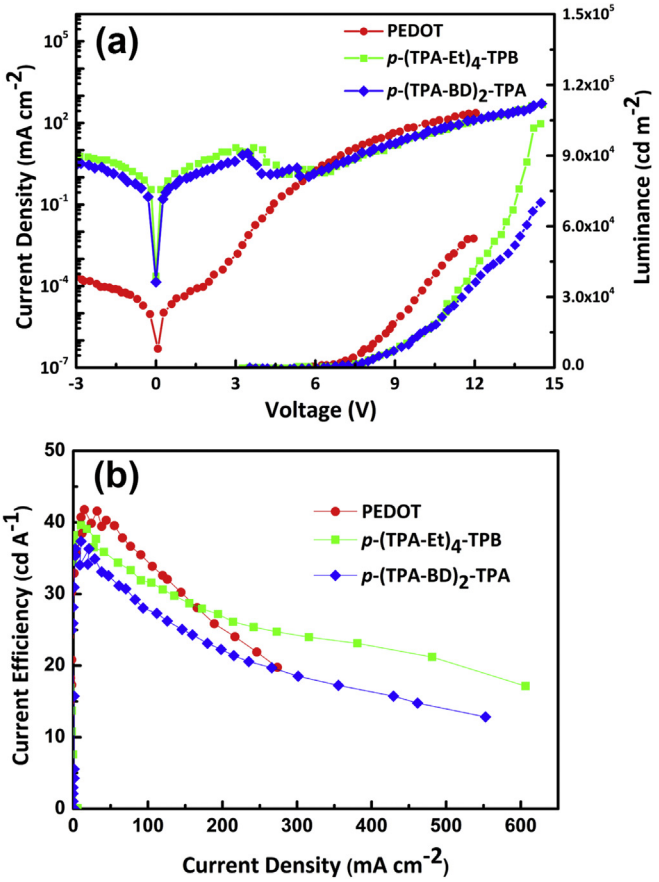

Fig. 8. The current density–voltage–luminance (J–V–L) curves (a) and current efficiencies-current density (b).

Another obvious improvement with p-(TPA-Et)$_4$-TPB and p-(TPA-BD)$_2$-TPA as HTL is maximum luminance (L_{max}). The OLEDs based on p-(TPB-Et)$_4$-TPB showed L_{max} of 103,690 cd m^{-2}, which was much larger than OLEDs based on PEDOT:PSS (L_{max} of 55,219 cd m^{-2}). This should be attribute to the LUMO level of p-(TPA-Et)$_4$-TPB (−2.41 eV) is higher than that of p-PPV (−2.90 eV). The p-(TPA-Et)$_4$-TPB can act as electron-blocking layer effectively (See Fig. 9).

However, when the OLEDs are operated at the low voltage region (5–12 V), the luminance of device-PEDOT is higher than device-p-(TPA-BD)$_2$-TPA and device-p-(TPA-Et)$_4$-TPB. As shown in Table 2, the

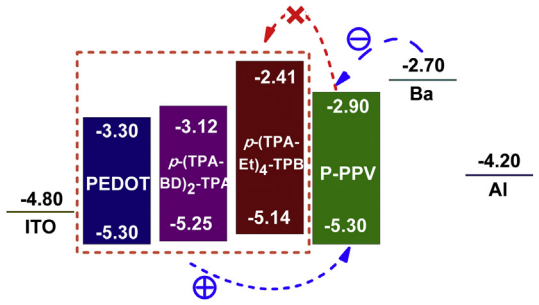

Fig. 9. Energy band diagrams of PEDOT, p-(TPA-Et)$_4$-TPB, p-(TPA-BD)$_2$-TPA and p-PPV.

maximum luminance efficiency (LE_{max}) of device-PEDOT is higher than OLEDs with as-synthesized HTMs. This phenomenon result in the smaller hole mobility (μ_{hole}) of as-synthesized HTMs (1.47×10^{-3} cm^2 V^{-1} s^{-1} for p-(TPA-BD)$_2$-TPA and 3.41×10^{-4} cm^2 V^{-1} s^{-1} for p-(TPA-Et)$_4$-TPB, measured by time-of-flight (TOF) technique under the fields of 2.0×10^5 V cm^{-1} at room temperature, ESI Fig. S7) than PEDOT (1.0×10^{-1} cm^2 V^{-1} s^{-1}) [36]. The electron-blocking effect of p-(TPA-Et)$_4$-TPB let the Device-p-(TPA-Et)$_4$-TPB having higher LE_{max} and larger L_{max} than device-p-(TPA-BD)$_2$-TPA, despite of the smaller μ_{hole}.

From Fig. 8, we noticed that the device-p-(TPA-BD)$_2$-TPA and device-p-(TPA-Et)$_4$-TPB showed L_{max} at 14 V, while the L_{max} of device-PEDOT is at 12 V. As reported, the PEDOT colloid solution is acid. During spin-coating, the indium ion will be mixed into the PEDOT layer. When the device operating, the indium ion will transfer to the EL and quench exciton [37]. Apparently, p-(TPA-Et)$_4$-TPB and p-(TPA-BD)$_2$-TPA as HTL can solve this problem.

As shown in the luminance efficiency (LE) vs. current density curves (Fig. 8b), the device-PEDOT showed more serious decrease of LE with higher operation current density than device-p-(TPA-BD)$_2$-TPA and device-p-(TPA-Et)$_4$-TPB. The stability at high operation current density can be quantified by the critical current density J_0, that is, the current at which the LE drops to half of its maximum value [38]. As shown in Table 2, the J_0 of PEDOT appeared at 256 mA cm^{-2}, while the J_0 of p-(TPA-BD)$_2$-TPA and p-(TPA-Et)$_4$-TPB appeared at 311 and 517 mA cm^{-2}, respectively, which indicated the improvement of stability with as-synthesized HTMs, and device-p-(TPA-Et)$_4$-TPB have shown a larger LE than device-PEDOT with operation current > 165 mA cm^{-2}, which might be due to the effect of indium ions we discussed above. In device-p-(TPA-BD)$_2$-TPA and device-p-(TPA-Et)$_4$-TPB, the efficiency at high operation current density was improved.

Table 2
The photoelectric properties of devices.

Device	V_{onset}[a] (V)	$\triangle E_{inj}$[b] (eV)	L_{max}[c] (cd m^2)	LE[d] (cd A^{-1})				J_0[e] (mA cm^{-2})
				LE_{max}[f]	LE_{150}[g]	LE_{200}[h]	LE_{250}[i]	
PEDOT	3.75	0.50	55,219	41.96	29.69	24.90	21.47	256.51
p-(TPA-BD)$_2$-TPA	3.50	0.35	70,941	36.36	24.77	22.12	20.27	311.22
p-(TPA-Et)$_4$-TPB	3.25	0.34	103,690	39.98	29.02	26.76	25.45	517.67

[a] V_{onset} = voltage at 1 cd m^{-2}.
[b] $\triangle E_{inj} = |HOMO_{HTL} - 4.80|$.
[c] Maximum luminance and the corresponding voltage.
[d] Luminance efficiency.
[e] J_0 = the current density at which the LE drops to 50% of its maximum value.
[f] Maximum luminance efficiency.
[g] Luminance efficiency at 150 mA cm^{-2}.
[h] Luminance efficiency at 200 mA cm^{-2}.
[i] Luminance efficiency at 250 mA cm^{-2}.

4. Conclusions

In this work, two HTMs *p*-(TPA-BD)$_2$-TPA and *p*-(TPA-Et)$_4$-TPB were synthesized as HTMs used in solution-processable FOLEDs. Both *p*-(TPA-BD)$_2$-TPA and *p*-(TPA-Et)$_4$-TPB can form free-standing films on the ring with diameter of 4 mm. The spin-coated films of *p*-(TPA-BD)$_2$-TPA and *p*-(TPA-Et)$_4$-TPB on PET-ITO substrates showed unobvious mechanical failure after bended with radius of curvature < 6 mm. These results demonstrate the outstanding film-forming capability of as-synthesized HTMs. The OLEDs with as-synthesized HTMs as hole injection and transport layer (HIL and HTL) showed an improvement of L_{max} and stability at higher operation current density, compared with commercialized PEDOT:PSS. The device with *p*-(TPA-Et)$_4$-TPB as HTL showed an maximum luminance levels of 103,690 cd m^{-2}, in which the *p*-(TPA-Et)$_4$-TPB layer showed an double function both as hole transporting and electron blocking.

Acknowledgments

The authors gratefully acknowledge the financial support from National High-tech R&D Program (2015AA033402) and Tianjin Science and Technology plan projects (13ZCZDGX00900).

Appendix A. Supplementary data

Supplementary data related to this article can be found at http://dx.doi.org/10.1016/j.dyepig.2015.10.004.

References

[1] Kim K, Kim SY, Lee JL. Flexible organic light-emitting diodes using a laser lift-off method. J Mater Chem C 2014;2:2144–9.
[2] Liu SH, Liu WB, Yu J, Zhang W, Zhang LT, Wen XM, et al. Silver/germanium/silver: an effective transparent electrode for flexible organic light-emitting devices. J Mater Chem C 2014;2:835–40.
[3] Wang XL, Shi GQ. Flexible graphene devices related to energy conversion and storage. Energy Environ Sci 2015;8:790–823.
[4] Ying L, Ho C-L, Wu HB, Cao Y, Wong W-Y. White polymer light-emitting devices for solid-state lighting: materials, devices, and recent progress. Adv Mater 2014;26:2459–73.
[5] Yang XL, Zhou GJ, Wong W-Y. Recent design tactics for high performance white polymer light-emitting diodes. J Mater Chem C 2014;2:1760–78.
[6] Tang CW, VanSlyke SA. Organic electroluminescent diodes. Appl Phys Lett 1987;51:913–5.
[7] Koishikawa Y, Miyazaki H, Yahiro M, Adachi C. Multi-layered organic light-emitting diode fabrication using low molecular weight materials by electrospray method. Thin Solid Films 2013;545:527–32.
[8] Cao XB, Wen YG, Guo YL, Yu G, Liu YG, Yang LM. Undoped, red organic light-emitting diodes based on a N,N,N′,N′-tetraphenylbenzidine (TPD) derivative as red emitter with a triphenylamine derivative as hole-transporting layer. Dyes Pigm 2010;84:203–7.
[9] Liang JJ, Li L, Niu XF, Yu ZB, Pei QB. Fully solution-based fabrication of flexible light-emitting device at ambient conditions. J Mater Chem C 2013;117:16632–9.
[10] Wong W-Y, Ho C-L. Functional metallophosphors for effective charge carrier injection/transport: new robust OLED materials with emerging applications. J Mater Chem 2009;19:4457–82.
[11] Wong W-Y, Ho C-L. Heavy metal organometallic electrophosphors derived from multi-component chromophores. Coord Chem Rev 2009;253:1709–58.
[12] Niu YH, Liu MS, Ka JW, Bardeker J, Zin MT, Schofield R, et al. Crosslinkable hole-transport layer on conducting polymer for high-efficiency white polymer light-emitting diodes. Adv Mater 2007;19:300–4.
[13] Lim Y, Park YS, Kang Y, Jang do Y, Kim JH, Kim JJ, et al. Hole injection/transport materials derived from Heck and sol-gel chemistry for application in solution-processed organic electronic devices. J Am Chem Soc 2011;133:1375–82.
[14] Forrest SR. The path to ubiquitous and low-cost organic electronic appliances on plastic. Nature 2004;428:911–8.
[15] Thelakkat M, Schmidt H-W. Synthesis and properties of novel derivatives of 1,3,5-tris(diarylamino)benzenes for electroluminescent devices. Adv Mater 1998;10:219–23.
[16] Zhu DX, Ye H, Zhen HY, Liu X. Improved performance in green light-emitting diodes made with CdSe-conjugated polymer composite. Synth Met 2008;158:879–82.
[17] Madan S. Color tuning and improved performance of poly[2-methoxy-5-(2′-ethyl-hexyloxy)-1,4-phenylenevinylene]-based polymer light emitting diode using cadmium selenide/zinc sulphide core shell uncapped quantum dots as dopants. J Nanophot 2011;5. 053518–8.
[18] Groenendaal LB, Jonas F, Freitag D, Pielartzik H, Reynolds JR. Poly(3,4-ethylenedioxythiophene) and its derivatives: past, present, and future. Adv Mater 2000;12:481–94.
[19] Kim J-S, Ho PKH, Murphy CE, Seeley AJAB, Grizzi I, Burroughes JH, et al. Electrical degradation of triarylamine-based light-emitting polymer diodes monitored by micro-Raman spectroscopy. Chem Phys Lett 2004;386:2–7.
[20] Gao WZ, Wang SR, Xiao Y, Li XG. Study on synthesis and properties of novel luminescent hole transporting materials based on N,N′-di(p-tolyl)-N,N′-diphenyl-1,1′-biphenyl-4,4′-diamine core. Dyes Pigm 2013;97:92–9.
[21] Zeng WJ, Wu HB, Zhang C, Huang F, Peng JB, Yang W, et al. Polymer light-emitting diodes with cathodes printed from conducting Ag paste. Adv mater 2007;19:810–4.
[22] Fulda KU, Tieke B. Langmuir films of monodisperse 0.5 μm spherical polymer particles with a hydrophilic shell. Adv Mater 1994;6:288–90.
[23] Li KP, Qu JL, Xu B, Zhou YH, Liu LJ, Peng P, et al. Synthesis and photovoltaic properties of novel solution-processable triphenylamine-based dendrimers with sulfonyldibenzene cores. New J Chem 2009;33:2120–7.
[24] Jolt Oostra A, Blom PWM, Michels JJ. Prevention of short circuits in solution-processed OLED devices. Org Electron 2014;15:1166–72.
[25] Gao WZ, Wang SR, Xiao Y, Li XG. Synthesis and properties of new luminescent hole transporting materials containing triphenylamine and carbazole units. Spectrochim Acta Part A 2012;98:215–21.
[26] Wu CS, Fang SW, Chen Y. Solution-processable hole-transporting material containing fluorenyl core and triple-carbazolyl terminals: synthesis and application to enhancement of electroluminescence. Phys Chem Chem Phys 2013;15:15121–7.
[27] Yasuhiko S, Hiroshi K. Charge carrier transporting molecular materials and their application in devices. Chem Rev 2007;107:953–1010.
[28] Wang JJ, Wang SR, Li XG, Zhu LF, Meng QB, Xiao Y, et al. Novel hole transporting materials with a linear π-conjugated structure for highly efficient perovskite solar cells. Chem Commun 2014;50:5829–32.
[29] Nakahara K, Mitsui C, Okamoto T, Yamagishi M, Matsui H, Ueno T, et al. Furan fused V-shaped organic semiconducting materials with high emission and high mobility. Chem Commun 2014;50:5342–4.
[30] Dandrade B, Datta S, Forrest S, Djurovich P, Polikarpov E, Thompson M. Relationship between the ionization and oxidation potentials of molecular organic semiconductors. Org Electron 2005;6:11–20.
[31] Wu HB, Huang F, Mo YQ, Yang W, Wang DL, Peng JB, et al. Efficient electron injection from a bilayer cathode consisting of aluminium and alcohol-/water-soluble conjugated polymers. Adv Mater 2004;16:1826–30.
[32] Mäkinen AJ, Hill IG, Kinoshita M, Noda T, Shirota Y, Kafafi ZH. Molecular engineering versus energy level alignment: interface formation between oligothiophene derivatives and a metal substrate studied with photoemission spectroscopy. J Appl Phys 2002;91:5456–61.
[33] Lewis J. Material challenge for flexible organic devices. Mater Today 2006;9:38–45.
[34] Ouyang X-H, Zeng H-P, Ding G-Y, Jiang W-L, Li J. Luminance materials containing carbazole and triphenylamine exhibiting high hole-transporting properties. Synth Met 2009;159:2063–9.
[35] Lin W-C, Lin H-W, Mondal E, Wong K-T. Efficient solution-processed green and white phosphorescence organic light-emitting diodes based on bipolar host materials. Org Electron 2015;17:1–8.
[36] Park J-Y, Kim JM, Lee H, Ko K-Y, Yook KS, Lee JY, et al. Thermally stable triphenylene-based hole-transporting materials for organic light-emitting devices. Thin Solid Films 2011;519:5917–23.
[37] Jo SJ, Kim CS, Kim JB, Ryu SY, Noh JH, Baik HK, et al. Increase in indium diffusion by tetrafluoromethane plasma treatment and its effects on the device performance of polymer light-emitting diodes. J Appl Phys 2008;103:114502.
[38] Murawski C, Leo K, Gather MC. Efficiency roll-off in organic light-emitting diodes. Adv Mater 2013;25:6801–27.